Journal of Materials Chemistry C

ROYAL SOCIETY OF CHEMISTRY

PAPER

View Article Online
View Journal

Cite this: DOI: 10.1039/d2tc04106e

Light-responsive bent-core liquid crystals as candidates for energy conversion and storage†

Ivan Dominguez-Candela, [abc] Iman Zulkhairi,[a] Inmaculada Pintre,[d] Nurul Fadhilah Kamalul Aripin,[ef] Jaime Lora-Garcia,[b] Vicent Fombuena,[c] M. Blanca Ros [d] and Alfonso Martinez-Felipe *[ag]

We have assessed the potential of light-responsive bent-core liquid crystals as candidate materials for energy conversion and storage applications. Samples comprise two chromophore bent-core compounds containing either one (IP33) or two (IP31) azobenzene groups, and their 5% (molar) mixtures with one non-chromophore bent-core compound (NG75), which was also measured as a reference material. The pristine compounds and their mixtures were introduced in thin transparent Indium Tin Oxide (ITO) cells, and were characterised by polarised optical microscopy, UV-visible spectrophotometry, impedance spectroscopy, and ferroelectric analysis, under different conditions of electrical fields and UV irradiation. All materials display smectic C polar phases (SmCP) except IP31, which forms columnar phases (Col), and IP33, IP31 and their mixtures exhibit light-responsiveness when irradiated at 365 nm due to reversible *trans*-to-*cis* photoisomerisation of the azobenzene units. All the bent-core based materials exhibit, at least, two dielectric relaxations, associated with different modes of molecular reorientation under weak alternating electrical fields (1 V_{rms}), as well as ferroelectric response that leads to permanent polarisation under the application of strong alternating fields (~75 kV cm^{-1}) at frequencies associated with the Goldstone-mode (1 Hz). Samples show considerable conductivity values and relaxor behaviour for liquid crystals, which can be tuned by application of UV light. In addition, we have induced in IP31 isothermal phase transitions from columnar to smectic phases (*via* the isotropic melt), by a combination of light and electrical stimuli. Our results confirm the potential of these bent-core compounds as light-harvesters for energy applications.

Received 28th September 2022,
Accepted 14th November 2022

DOI: 10.1039/d2tc04106e

rsc.li/materials-c

1. Introduction

The development of innovative electrolytes that can improve the efficiency of renewable energy conversion and storage will play a decisive role to reduce greenhouse emissions and reach net-zero targets globally.[1] Liquid crystals hold promise as advanced materials in different renewable technologies, due to their ability to interact with, and respond to, external sources, resulting in tailor-made nanostructures.[2–4] More specifically, azobenzene-containing compounds can exhibit liquid crystalline phases controllable by light excitation, *via trans*-to-*cis* photoisomerisation. In its ground state, the azobenzene *trans* isomer is linear, and hence compatible with liquid crystalline phases, since it tends to promote order and interactions in the mesophase range. When excited with UV light at certain frequencies, the *trans*-isomer bends, normally disrupting the liquid crystal order. Even though azobenzenes have been studied for several decades,[5–7] they continue to attract interest due to their potential to promote long-range macroscopic changes induced by short-range molecular modifications.[8–12]

Bent-core liquid crystals, BCLCs, exhibit anti-ferroelectric and ferroelectric behaviour with high figures of merit, which can be useful for energy storage applications. BCLCs can form columnar (Col, former B_1), polar smectic C (SmCP, former B_2), twist grain boundary dark conglomerate (DC) or helical

[a] Chemical Process and Materials Research Group, School of Engineering, University of Aberdeen, King's College, Aberdeen AB24 3UE, Scotland, UK. E-mail: a.martinez-felipe@abdn.ac.uk
[b] Instituto de Seguridad Industrial, Radiofísica y Medioambiental (ISIRYM) Universitat Politècnica de València (UPV), Plaza Ferrándiz y Carbonell, s/n 03801 Alcoy, Spain
[c] Technological Institute of Materials (ITM), Universitat Politècnica de València (UPV), Plaza Ferrándiz y Carbonell 1, 03801 Alcoy, Spain
[d] Instituto de Nanociencia y Materiales de Aragón, Departamento de Química Orgánica, Facultad de Ciencias, Universidad de Zaragoza-CSIC, Campus San Francisco, E-50009 Zaragoza, Spain
[e] School of Chemical Engineering, College of Engineering, Universiti Teknologi MARA, 40450 Shah Alam, Selangor, Malaysia
[f] Department of Chemistry, School of Natural and Computing Sciences, University of Aberdeen, King's College, Aberdeen AB24 3UE, Scotland, UK
[g] Centre for Energy Transition, University of Aberdeen, King's College, Aberdeen AB24 3UE, Scotland, UK

† Electronic supplementary information (ESI) available. See DOI: https://doi.org/10.1039/d2tc04106e

nanofilament (HNF, former B_4) phases among others.[13–20] Generally, BCLC molecular designs show several aromatic rings forming an angle through a central meta-substituted ring (which facilitates molecular packing), various linking groups, and flexible terminal chains at one or both end of the molecule (which reduce the melting point). The bent-core mesogenic units lead to biaxial properties, and the relative orientation of polar groups present at the core respect to the molecular axes promotes the appearance of local dipole moments. Upon application of electric fields, the cooperative alignment of these dipoles can result in local (within the liquid crystalline regions or layers) and macroscopic (through the material) polarisation, which can be further maintained if the viscous forces are strong enough once the field is removed.[21,22]

In this work, we combine the application of electric fields and light to explore new phenomena in BLCSs that can lead to energy conversion and storage from solar sources.[23–27] We analyse the photo-dielectric and photo-ferroelectric response of bent-core liquid crystals containing azobenzenes as chromophore groups. We also investigate the photoinduction of isothermal phase transitions in the materials, as a mechanism to control the nanostructure of future electrolytes.

2. Experimental section

2.1. Materials and cells preparation

Five materials were studied in this work. Three pristine bent-core compounds were used, containing six aromatic rings at the core, which is linked to long flexible chains ($-OC_{14}H_{29}$). The pristine materials already reported by us are designated as: NG75 (non-chromophore), IP31 (containing two azobenzene groups), and IP-33 (containing one azobenzene group), see Fig. 1. Their synthesis and full characterisation are described in detail elsewhere, and are summarised as Electronic Supplementary Information, see Table S1 (ESI†)[28–30] In short, NG75 and IP33 display smectic C polar phases (SmCP), and IP31 shows a columnar phase (Col). Additionally, two mixtures, containing NG75 (95%, molar) and either IP33 or IP31 (5% molar, each), were prepared by melting above the clearing temperatures of the respective compounds. The choice of composition was based on some of our previous results obtained for liquid crystal dimers, which showed that 5% molar was the minimum concentration of azobenzene molecules required to promote photoinduced effects in the corresponding mixtures.[31]

The pristine materials and the mixtures were filled from their melt into commercial ITO-coated (Indium Tin Oxide) glass cells (SG100A080uG180, Instec) by capillary action, using a Linkam TM600 hot stage, see Fig. S1 (ESI†). Cells have an active area of $A = 100\ mm^2$, thickness of $h = 8\ \mu m$, resistance of 100 Ω, and their overall capacitance, C_0 can be calculated as:

$$C_0 = \frac{\varepsilon_0 A}{h} = 1.11 \times 10^{-10} F \quad (1)$$

with $\varepsilon_0 = 8.854 \times 10^{-12}\ F\ m^{-1}$ is the permittivity of vacuum. The ITO cells were then connected to the different analysers using two aluminium foils attached to the sides of the glass cells with RS PRO conductive silver paint.

2.2. Characterisation techniques

Temperature was controlled by placing the cells on top of a Linkam THMS 600 heating stage coupled to a TMS 91 control unit, with ±0.1 °C accuracy. For phase observation, the heating stage was placed on an Olympus Bx5m polarised optical microscope, POM, equipped with cross polarisers. Phase behaviour was further assessed by differential scanning calorimetry, DSC, using a Mettler Toledo QA200 calorimeter. The thermograms were obtained in heating, cooling, and reheating cycles, at ±10 °C min^{-1} rates, under inert (N_2) atmosphere. Complex impedance spectroscopy was carried out using the Solartron Modulab XM frequency response analyser (FRA). Frequency

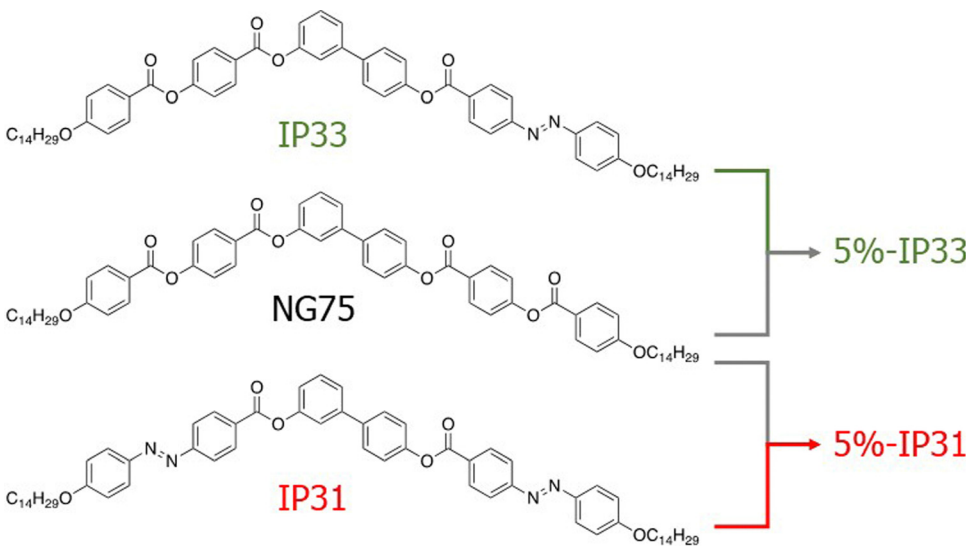

Fig. 1 Chemical structure and notation used to refer to the pristine bent-core compounds (NG75, IP33 and IP31) and mixtures containing 5% molar % of azobenzene molecules (5%-IP33 and 5%-IP31).

sweeps ranged from 0.01 to 10^6 Hz, using alternating fields of 1 V_{rms} amplitude; some additional isothermal experiments were taken at a fixed frequency of 1 Hz, in the time domain. The ferroelectric response was analysed by a RT66C Test System (Radiant Inc), by measuring the polarisation of the cells, through hysteresis loops of sinusoidal fields in the $\pm$75 kV cm^{-1} range, and at different frequencies.

The effect of UV irradiation was investigated using a Dymax Bluewave QX4 TM LED pot-curing system, controlled by a Dymax ACCU-CALTM 50-LED instrument. Samples were irradiated at 365 nm, at different light intensities (up to 1200 mW cm^{-2}) measured with a detector. The UV-vis spectra of the materials were collected for tetrahydrofuran (THF) solutions, or for thin films cast on quartz slides. Selected samples were irradiated with UV light (365 nm, 260 mW cm^{-2}), and the UV-visible spectra were obtained as a function of exposure and relaxation time, using a VARIAN Cary 50 Scan UV-vis spectrophotometer, between 250 nm and 550 nm. Additional dielectric and ferroelectric measurements were carried under the application of different programs of UV light irradiation, using the Dymax Bluewave QX4 TM LED pot-curing system. Most of these experiments were carried out at a fixed intensity of 200 mW cm^{-2}, but further details on the experimental conditions are given below at the respective sections.

3. Results and discussion

3.1. Phase behaviour

The thermal properties of the pristine compounds and the 5% mixtures inside the ITO cells are summarised in Table 1, based on POM observations. NG75 and IP33 display granulated textures, see Fig. 2(a) and (b), which are consistent with the formation of liquid crystalline smectic C (SmC) phases. More specifically, both compounds were assigned to form smectic C antiferroelectric polar (anticlinic) phases, SmC_AP_A,[28,29,32,33] which were confirmed by ferroelectric experiments. IP31, on the other hand, shows banana leaf textures, consistent with the formation of oblique columnar phases, Col_{ob}, Fig. 2(c).[28] The thermal behaviour of the three pristine compounds is also in good agreement with DSC measurements on their respective powder samples, see Fig. S2 (ESI†) and Table 1. We attribute minor temperature value deviations to heat transfer and potential anchoring effects with the ITO cells surfaces. As expected, the 5% mixtures (5%-IP31 and 5%-IP33) exhibit similar microscopic textures as NG75 (95% molar), which confirms the formation of SmC polar (SmCP) phases in comparable temperature ranges, Fig. 2(d) and (e).

3.2. Dielectric analysis

The dielectric responses of NG75, IP31, IP33 and their mixtures (5%-IP31 and 5%-IP33) are summarised in Fig. 3, where we show 3D-plots of their dielectric loss factor (ε'', relative to ε_0) as a function of frequency and temperature. Their isothermal 2D curves used to prepare these 3D graphs, as well as the plots for the dielectric elastic constant, ε' (relative to ε_0), and the real component of the complex conductivity, σ', can be found as supplementary information (Fig. S3–S5, ESI,† resp.). NG75 displays several dielectric processes in Fig. 3(a), which we have initially labelled as γ, β and α, in increasing temperature order. At sufficiently high temperatures, the rise of ε'' observed at low frequencies is attributed to the existence of strong direct current (dc) conductivity between the electrodes, σ_{dc}.[34] Since the low-temperature process (γ) appears in a very narrow frequency range at very low temperatures, and seems to be associated to the crystal phase, we will focus on the higher temperature processes.

Table 1 Thermal parameters obtained for the bent-cores by differential scanning calorimetry (DSC), measured on second heating (10 °C min^{-1}) scans, and by polarised optical microscopy (POM) measured on cooling (1 °C min^{-1})

	DSC		POM	
Sample	T_{Cr-M}/°C (ΔH_{Cr-M} (kJ mol^{-1}))	T_{M-I}/°C (ΔH_{M-I} (kJ mol^{-1}))	T_{I-M}/°C	T_{M-Cr}/°C
NG75	77.2 (13.74)	159.7 (24.76)	161.6	—[a,b]
IP33	118.4 (58.05)	163.3 (25.55)	163.6	110.0[b]
IP31	139.9 (31.30)	168.3 (21.08)	170.5	134.9[c]
5%-IP33	75.1 (15.89)[d]	156.2 (20.08)[d]	161.8	—[a,b]
5%-IP31	74.0 (15.50)[d]	153.6 (18.77)[d]	161.8	—[a,b]

[a] Not visible under POM. Crystallisation was further confirmed under dielectric measurements. Cr: crystal; M: mesophase ([b] SmCP, [c] Col); I: isotropic liquid; ΔH: enthalpy; T: transition temperature. [d] Enthalpy values were calculated using the molecular weight of NG75.

Both α and β are well-defined in the smectic materials, Fig. 3(a), (b), (d) and (e), and shift towards lower frequencies on cooling, suggesting these are dielectric relaxations. In order to discriminate their molecular origin, we have superimposed direct current electric fields of different intensities (0.5 to 4 V) to the alternating field ($\pm$1 V_{rms}) and measured ε'' in similar frequency sweeps as in Fig. 3. The results for NG75 are illustrated in Fig. 4 and show that the low-frequency relaxation (α) decreases and shifts to lower frequencies at increasing dc fields. This phenomenon is typical of a Goldstone(phason)-mode relaxation, which involves cooperative motions of the molecules within the smectic layers, albeit without varying the tilt angle.[35–38] The application of dc electric fields perturbs the cooperative interactions and then the relaxation is suppressed. The β process of NG75 at higher frequencies, on the other hand, remains unaffected upon dc electric fields, and can be associated to a soft(amplitude)-mode relaxation, when molecules vary their tilt angle, θ, within the same plane. IP33 shows similar dielectric relaxations and comparable dielectric response as NG75, Fig. 3(b).

IP31, on the other hand, displays the dielectric regions discussed above, even though the α process is less defined than in the smectic materials, Fig. 3(c). This may be due to the existence of strong constrains to reorient molecules within columnar structures. On applying dc electrical fields, the β process of IP31 is enhanced, see Fig. S6 (ESI†), which is accompanied with a slight displacement of its maxima. Therefore, the molecular origin of the β relaxation must be different in IP31, and this is confirmed by its higher activation energy, E_a, compared to NG75 and IP33, see Fig. 5. A process in a similar frequency/temperature range was identified previously for bent-cores containing sulphur atoms, and was attributed to the

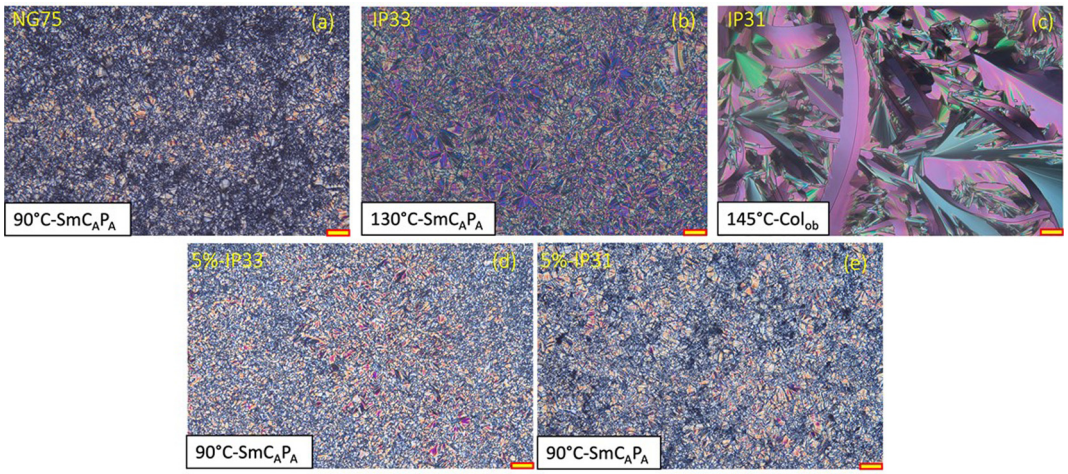

Fig. 2 Selected polarised optical microphotographs showing the mesophases displayed by the pristine bent-core compounds (a, b and c) and the mixtures containing 5% of IP33 (d) and IP31 (e). Scale bar corresponds to 40 μm. SmC$_A$P$_A$: smectic C antiferroelectric polar (anticlinic); Col$_{ob}$: oblique columnar.

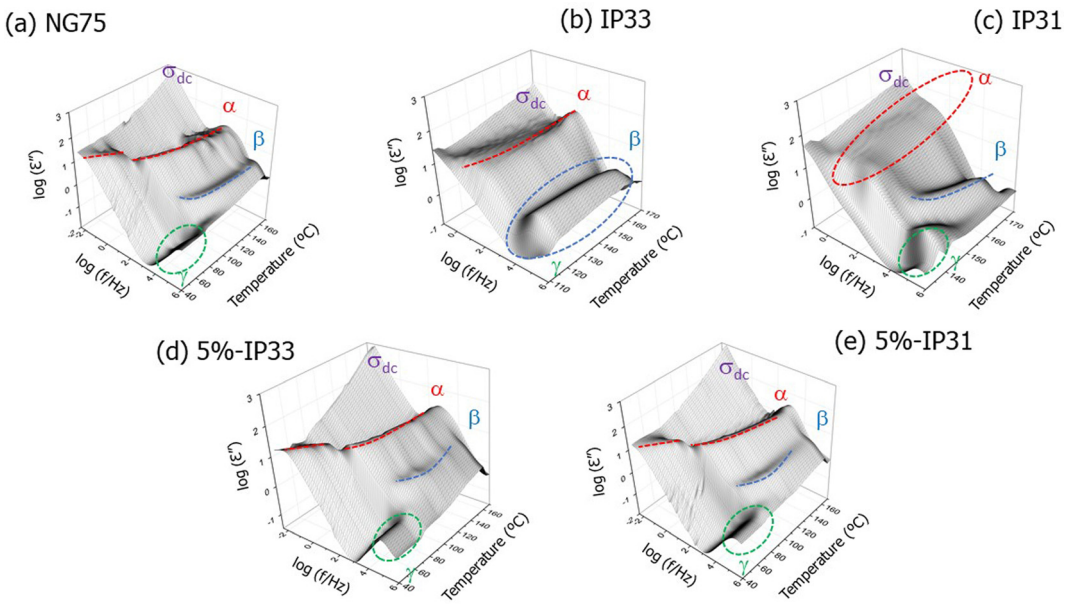

Fig. 3 3D-plots showing the dielectric loss factor, ε'', as a function of frequency and temperature, corresponding to: (a) NG75; (b) IP33; (c) IP31; (d) 5%-IP33; and (e) 5%-IP31, obtained in isothermal steps, on cooling from their isotropic phases.

rotation of the molecules around their molecular long axis.[39] The α process of IP31, appearing at lower frequencies, can be linked to longer-range phenomena probably involving macro dipole moments within the columns, which consequently shows very small temperature dependence.[40] Interestingly, the α region of IP31 decreases under the application of dc fields, even though it is not inhibited, unlike for NG75. This fact may reflect the stronger constrains for cooperative molecular motions (in response to dc fields) found in columnar nanostructures, compared to smectic phases.

As expected, the two mixtures depict a similar dielectric responses as NG75, Fig. 3(d) and (e), which is also consistent with their similar phase behaviour.[40] The Arrhenius plots corresponding to the maximum frequency of the ε'' peaks in both the α and β relaxations, f_{max}, deviate to some extent from linearity and follow Vogel–Fulcher–Tamman (VFT) behaviour, see Fig. 5. This indicates that the molecular motions within the smectic layers are controlled by viscous forces. The Goldstone-mode (α process in our notation) has activation energies in the 50 kJ mol^{-1} range in the mesophase, which is typical of locally activated rotation motions of rod-like molecules, previously observed in smectic liquid crystals.[41–44] Interestingly, the soft-mode (β process), has higher E_a values than the α relaxation, which reflects a stronger energy barrier for the bent-core molecules to modify their tilt angle, θ. These are still in the same range as other processes in smectic materials.[35] The

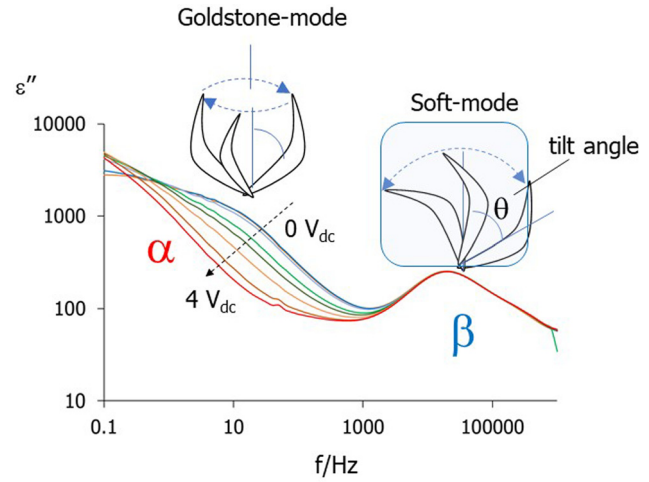

Fig. 4 Effect of direct current electrical fields of various amplitudes on the dielectric loss factor, ε'', measured in the smectic phase of NG75 (T = 90 °C), and assignation of the α and β relaxations to molecular modes.

higher activation energies estimated in the crystal phase indicate stronger interactions and mobility constrains due to the increase in order at lower temperatures.

The appearance of plateaus in the double logarithmic plots of the real component of the complex conductivity, σ', Fig. S5 (ESI†), denotes direct conductivity in the bent-core molecules, with σ_{dc} values in the 10^{-9} to 10^{-4} S cm^{-1} range. Even though these are much lower than those exhibited by benchmark electrolytes for batteries or fuel cells ($\sim 10^{-1}$ S cm^{-1}),[45,46] the occurrence of direct conductivity opens the opportunity to promote ionic mobility activated by molecular motions within liquid crystal structures.[47–56] It is also worth noting that, within the electric fields ranges applied (± 1 V_{rms}, 4 V), we did not observe noticeable textural changes in our samples under the microscope, and we will return to this observation later.

3.3. Ferroelectric response

We have assessed the ferroelectric response of our bent-core materials by applying strong alternating electrical fields (in the ± 75 kV cm^{-1} range) following triangular hysteresis loops, at different temperatures and frequencies. All samples exhibit non-linear polarisation response, and remanent polarisation (at zero voltage, P_r), typical of ferroelectric behaviour, which is illustrated for IP33 in Fig. 6.

The application of electrical fields in NG75 and IP33 (and 5%-IP33 and 5%-IP31) induces textural changes, which may indicate molecular rearrangements and polarisation within the smectic layers, but we could not find evidence of phase transitions. The absence of field-induced phase transitions in our samples is not surprising, since the threshold electrical field required to collapse the mesophase of these bent-core compounds are reported in the 100 kV cm^{-1} range,[29] which we could not reach due to experimental constrains. Dark conglomerate phases (DC) in NG75 were not observed either, which may be due to strong anchoring effects at the surface of our ITO cells. The columnar organisations of IP31 also remain during the hysteresis cycles, but some stripes appear in the banana leaves textures within the liquid crystal domains, particularly visible after several cycles and at low frequencies, Fig. S7(a)–(f) (ESI†). Similar features are also observed due to the appearance of lamellar (or pseudo-layered) organisations[57–59] or flexoelectric effects[60,61] in nematic phases. Even though SmCP structures can

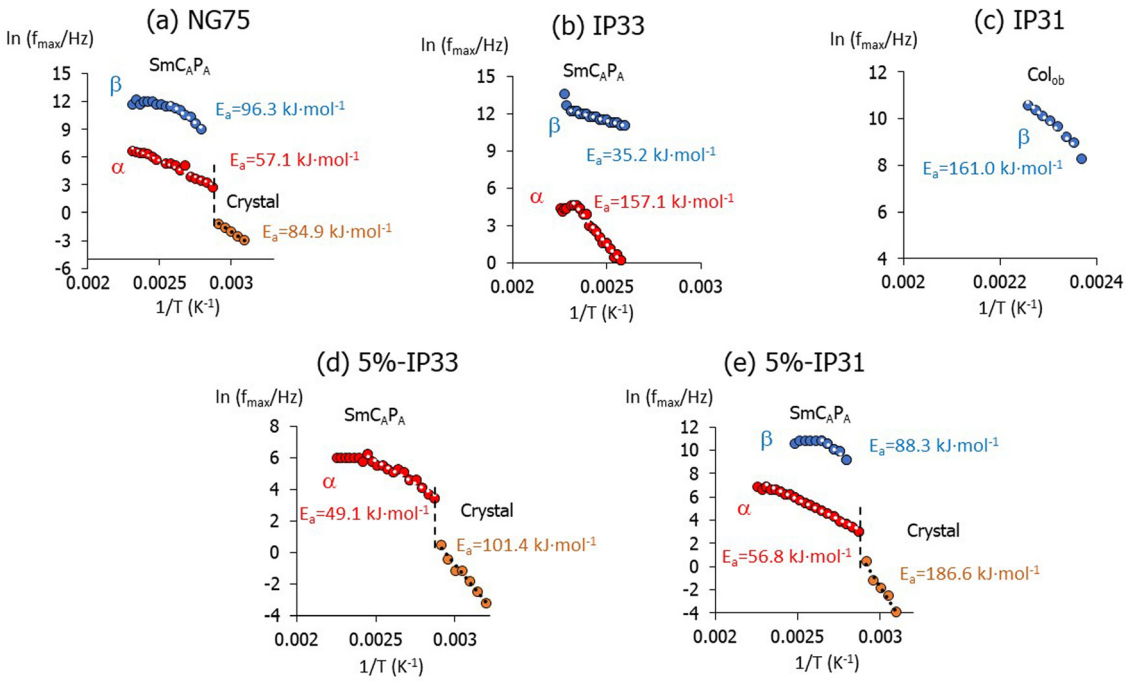

Fig. 5 Arrhenius plots obtained for the maxima (f_{max}) of the dielectric loss factor curves, ε'', and apparent activation energies, E_a, estimated for the α and β relaxations (see white points as selected linear regions). (a) NG75; (b) IP33; (c) IP31; (d) 5%-IP33; (e) 5%-IP31.

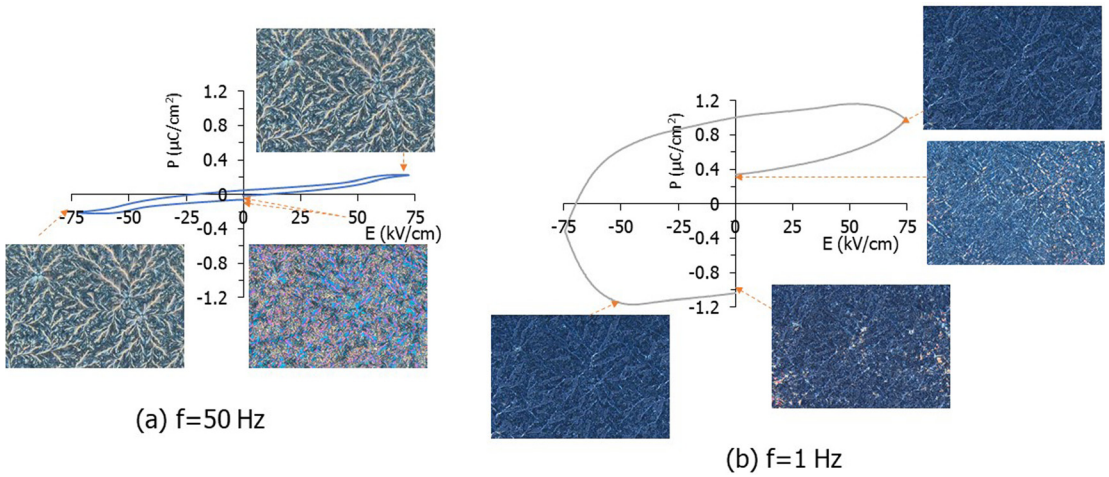

Fig. 6 Hysteresis loops and associated polarised optical micrographs showing the ferroelectric response of IP33 at: (a) 50Hz and (b) 1 Hz (T = 130 °C, SmCP phase).

develop from columnar phases in bent-core materials (inducing B1 to B2 phase transitions), this normally occurs if the sample is cooled down from the isotropic liquid, under application of low frequency alternating electrical fields.[28,62]

The values of remanent polarisation (P_r) and saturated polarisation (P_s, at the highest voltage), and the effects on textural changes, are more prominent at low frequencies where Goldstone-modes are prevalent, see Fig. S7 (ESI†). As expected, the ferroelectric response improves with temperature within the mesophase, see Fig. S8(b) (ESI†), attributed to the higher molecular mobility illustrated by the Arrhenius plots in Fig. 5. These dependences with temperature and frequency are comparable for the five samples under study. Polarisation values are within the range of other SmC materials ($\sim$0.5 μC cm^{-2}).[63]

Both 5%-IP33 and 5%-IP31 show ferroelectric response, and the introduction of the azobenzene compounds modifies the initial response of NG75 in the mixtures, with similar saturated polarisation values, P_s, but lower remanent polarisations, P_r, Table S2 (ESI†). Therefore, whilst the NG75 ferroelectric behaviour seems to be weakened, the mixtures gain in relaxor response and capacity to store energy (E_s, J cm^{-3}), calculated from the integrated area in the polarization-electric field (P-E) hysteresis loops, see Fig. S8(a) (ESI†). It is worth noting how the mixtures response is controlled by the azobenzene compounds, even though these only represent 5% of their overall molar composition. Despite the low energy values (8.79–9.28 mJ cm^{-3} range), compared to inorganic relaxors (180–4000 mJ cm^{-3} range[64,65]) these results illustrate the capacity of our mixtures (and pristine materials) to harvest energy.

3.4. Light response and light effect on the dielectric and conductivity response

Fig. 7(a) shows the UV-visible spectra of IP31, IP33, and their 5% mixtures in NG75, obtained in tetrahydrofuran (THF) solutions ($\sim 10^{-5}$ M) at room temperature. All solutions show one strong band centred at around $\sim$365 nm, due to the lowest-energy π* ← π transition in the *trans*-azobenzene isomer, and a much smaller intensity absorption peak in the visible region ($\sim$440 nm), assigned to a weak π* ← n transition in the *cis*-azobenzene.[66] Upon UV irradiation (365 nm; 260 mW cm^{-2}), the azobenzenes undergo *trans*-to-*cis* photo-induced isomerisation, evidenced by a decrease in the $\sim$365 nm band and a simultaneous (slight) increase of the $\sim$440 nm band, illustrated for IP31 in Fig. 7(b). When the solutions are kept in the dark after illumination, the UV-vis spectra recover

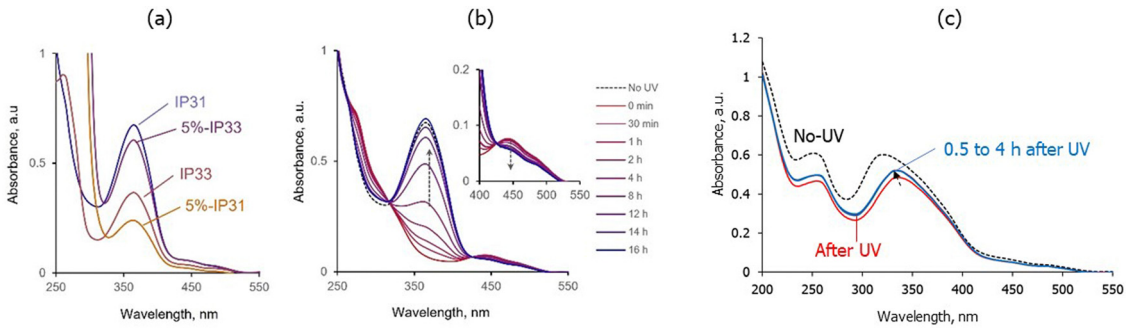

Fig. 7 UV-visible spectra of the light-responsive bent-core based samples: (a) IP33, IP31, 5%-IP33 and 5%-IP31 measured in $\sim 10^{-5}$ M THF solutions at room temperature (IP31 and IP33 : 1.2 × 10^{-5} M; 5%-IP31: 11.3 × 10^{-5} M; 5%-IP33: 37.8 × 10^{-5} M). IP31 spectra measured before and at different times after light irradiation (260 mW cm^{-2}; 365 nm): (b) in THF solution at room temperature; and (c) on a film cast on quartz at its mesophase (145 °C). Arrows in (b) and (c) indicate signal recovery after UV irradiation (t = 0 min) while samples were kept in the dark.

their initial shape (prior to UV illumination) before 24 hours after exposure, due to thermally induced *cis*-to-*trans* back-relaxation of the azobenzene groups,[67] see also Fig. S10 (ESI†). There are no significant differences in the range of back (thermal) isomerisation kinetics of the four solutions (compounds), which is illustrated by their half-live ($t_{1/2}$) values (between 4 and 6 hours) estimated from the maxima of the time-dependent curves, see Table S3 obtained from Fig. S11 (ESI†).

The UV-vis absorption spectra measured on quartz films (at the mesophase) show lower intensities than their respective THF solutions, probably due to their thicknesses, see Fig. 7(c) for IP31. Interestingly, the maxima of the absorbance peaks appear at lower wavenumbers (~325 nm), together with multiple shoulders. This response denotes the formation of azobenzene aggregates in the films, and more specifically, such low frequency values are consistent with predominant head-to-head stacking of aromatic rings to form H-aggregates.[68] Illumination of the films with a 365 nm UV source (260 mW cm^{-2}) promotes less acute changes in the curves than in solution, which could have a two-fold explanation. On the one hand, the high viscosity of the mesophase (consistent with the formation of H-aggregates) may inhibit some of the motions necessary for the *trans*-to-*cis* isomerisation.[42] On the other hand, at high temperatures the thermally activated *cis*-to-*trans* back-relaxation is favoured, displacing the equilibrium towards the formation of *trans* azobenzene isomers.[31] It is worth noting that the maxima of the absorption peak in Fig. 7(c) appears at larger wavelengths after irradiation. We hypothesize that this could be due to selective photoisomerization of the (predominant) H-aggregates in the films, while azobenzene groups arranged in head-to-tail arrangements (J-aggregates) seem to be less affected by UV-irradiation. We also note that, after 0.5 hours, the UV-vis signal does not change to a great extent during the whole experiment duration (4 hours). This behaviour could be useful for light-energy storage, even though we acknowledge that further time-dependent experiments will be necessary to confirm, and shed more light on, the mechanisms involved.

We have applied UV irradiation (365 nm) to control the dielectric response of the light-responsive bent-core based materials, and we illustrate some of these effects in Fig. 8, where we show the real component of their complex conductivity, σ', measured at their mesophases (T = 90 °C). Light irradiation (200 mW cm^{-2}) enhances σ' at lower frequencies, and such selective increase rules out mere thermal effects on the conductivity response. Interestingly, the rise in conductivity seems more effective in the smectic materials, *i.e.*, the 5% mixtures and IP33, Fig. 8(a), (c) and (d). We believe that the presence of *cis*-isomers may enhance the alignment of the layer(s) adjacent to the cells surfaces, facilitating long-range conductivity.[31] We cannot rule out, however, that continuous *trans*-to-*cis*-to-*trans* photoisomerisation, or the occurrence of iso-mesophase micro transitions, may also favour such alignment. As expected, similar irradiation doses have neglectable effects on the conductivity of NG75, see Fig. S12 (ESI†).

Most of these light-induced effects observed in the bent-core based materials are fully reversible and can be tuned to some extent by changing the experimental conditions. In Fig. S13 and S14 (ESI†) we display a selection of graphs that illustrate the

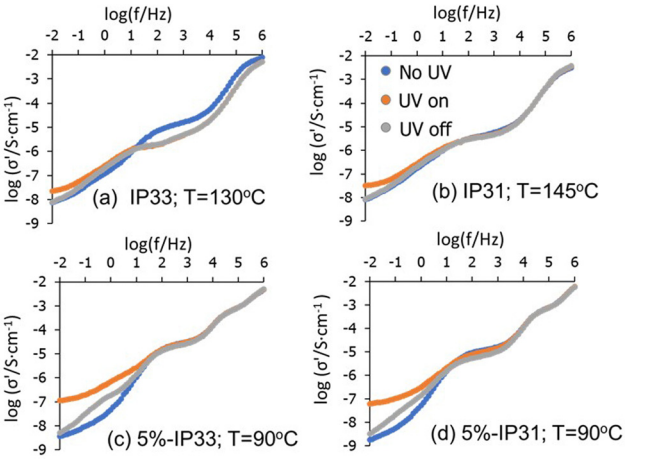

Fig. 8 Frequency dependence of the real component, σ', of the complex conductivity, σ^*, measured at the mesophases of the light-responsive bent-core based materials before (blue), during (orange) and after (grey) UV illumination (200 mW cm^{-2}; 365 nm).

effect of temperature on their dielectric loss factor, ε''. Even though a closer (and quantitative) inspection is out of the scope of this paper, the response seems to be favoured at medium-low temperatures within the mesophase. This observation seems consistent with the promotion of the *cis*-to-*trans* thermal relaxation at high temperatures, resulting in a less acute light-response.

The curves in Fig. 8 (and Fig. S13 and S14, ESI†) were taken after two minutes of light irradiation (and then cessation), but they do not capture the dynamics of the photoisomerisation process. Hence, we have monitored the time dependence of the dielectric elastic constant of our materials, ε', during irradiation cycles (T = 130 °C, 365 nm, and 200 mW cm^{-2}), at a fixed frequency of 1 Hz (for consistency with our ferroelectric results). Fig. 9 displays how irradiation promotes an almost immediate and linear rise in the ε' values (first step) followed by a slower increase to reach a plateau (second step). The first step can be linked to the fast *trans*-to-*cis* isomerisation of the azobenzene groups, initiated at the surface exposed to UV irradiation, with the bent geometry of the *cis*-azobenzenes further contributing to the local dipole moment of the bent-core molecule. The second step could be related to molecular reorganisations within the bulk of the mesophase, which further increase the dielectric response. These profiles agree with those obtained previously for other light-responsive liquid crystals.[69,70]

After UV light is switched off, the curves in Fig. 9 follow a similar, yet reversed and slower, two-step decrease: a fast drop in values followed by negative exponential decay until the initial ε' values are recovered asymptotically. These results are consistent with the curves in Fig. 8 and confirm that the processes have reached steady states long before 120 s (2 minutes), see Table S4 (ESI†). It is worth noting, however, that even though the responses from the four samples are comparable (all samples at 130 °C yield 95% of the final values under illumination after 28 s and recover 95% of the initial value after 40 s of UV cessation), the second step seems to be slightly slower in the 5% mixtures, compared to the response of the pristine IP33 and IP31. This opens the possibility

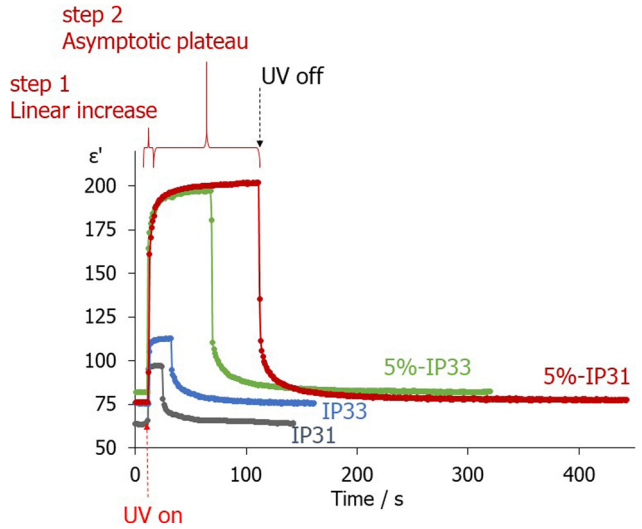

Fig. 9 Time-dependence of the dielectric elastic constant, ε', measured at 1 Hz and 160 °C (mesophases range) for the four light-responsive bent-cores under study, when submitted to UV off-on-off cycles (200 mW cm^{-2}; 365 nm). Arrows and steps correspond to 5%-IP31.

to control the dielectric properties *via* composition and promote storage effects with small amounts of light-responsive dopants.

4.5. Light irradiation under high voltages: isothermal phase transitions

Fig. 10 illustrates the effect of UV light during the application of ferroelectric hysteresis loops (±75 kV cm^{-1} range) measured at 1 Hz. Table 2 summaries the values obtained for P_s, P_R, energy stored and efficiency of energy storage (η) in the mesophase, estimated as:

$$\eta = E_S/(E_S + E_L) \quad (2)$$

corresponding to the fraction of energy stored (E_S) respect to the overall energy involved in the process (including the area within the hysteresis loop, E_L), highlighted in Fig. S8 (ESI†).

As expected, polarisation (P_s, P_R) increases for the samples during irradiation due to *trans*-to-*cis* isomerisation, which is consistent with the increase in ε' values in Fig. 9, whereas the curves tend to recover their initial values after UV is switched off. On the other hand, UV irradiation promotes lower E_S and higher E_L values in all samples, see Fig. 10, resulting in lower efficiencies, η. The reduction of E_S during UV irradiation could be attributed to a dissipation of certain amount of energy during reorientation of the azobenzene groups when UV is switched on, which results in higher E_L (broad hysteresis loop). Such energy effects can be particularly strong if the isomerisation mechanism involves rotational (non-planar) reconfigurations of the azobenzenes.[71]

Once irradiation is ceased, E_S and η increase for the four samples with a value higher than in the initial conditions, which is an interesting strategy to attain better capacity of dipole reorientation in cyclic processes. The η values (in the 0.198–8.49% range) are comparable to those reported by Kumar *et al.* for specific compositions of ceramics doped with zirconate titanate; the low efficiency was then attributed to domain wall movements that affected the main ferroelectric parameters.[72] As mentioned previously, whilst the E_s values in the mixtures are low (0.87–4.06 mJ cm^{-1}), the UV irradiation effect to the dipole reorientation (P_s, P_R) opens the possibility to moderate the hysteresis loop behaviour *via* UV irradiation.

As discussed above, the application of electrical fields (on its own) did not promote isothermal phase transitions in

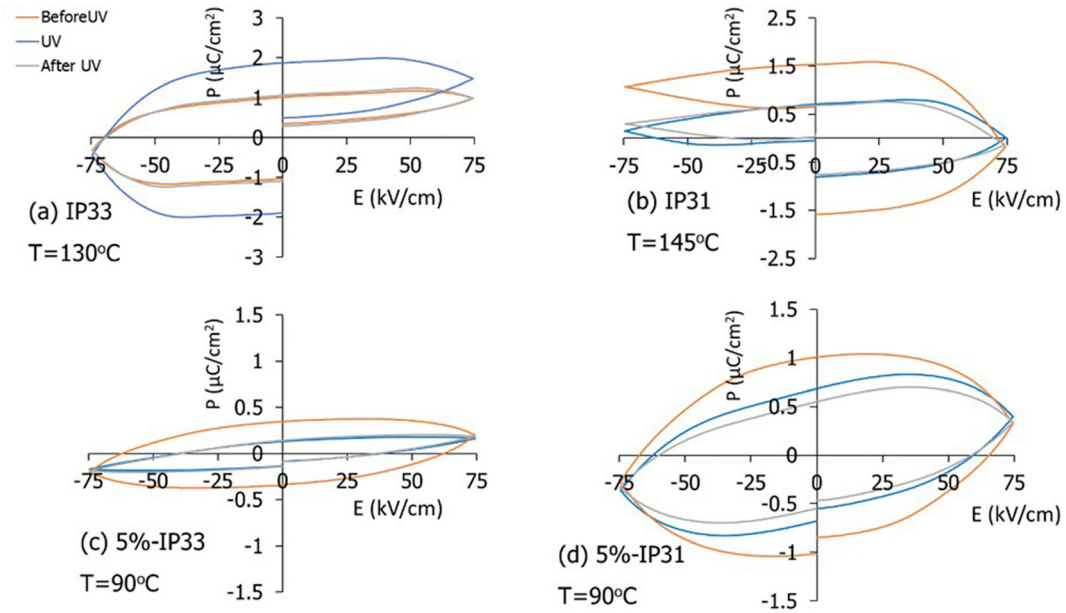

Fig. 10 Hysteresis loops showing the effect of light on the ferroelectric response for the samples containing azo-bent core molecules (values taken at 1 Hz in their mesophases). (a) IP33; (b) IP31; (c) 5%-IP33; (d) 5%-IP31.

Table 2 Values for saturated polarisation values, P_s, remanent polarisation, P_r, energy storage (E_s) and efficiency (η), as a function of UV light irradiation during 1 Hz ferroelectric loops, estimated at their respective mesophases: 130 °C (a); 145 °C (b); 90 °C (c and d)

	Before UV				During UV			
Sample	P_S (μC cm^{-2})	P_R (μC cm^{-2})	E_S (mJ cm^{-3})	η (%)	P_S (μC cm^{-2})	P_R (μC cm^{-2})	E_S (mJ cm^{-3})	η (%)
[a]IP33	0.979	1.012	6.91	6.63	1.479	1.875	4.23	1.37
[b]IP31	0.0149	0.711	3.52	5.26	−0.180	1.510	2.69	1.18
[c]5%-IP33	0.167	0.133	1.85	7.65	0.192	0.345	0.865	1.12
[d]5%-IP31	0.395	0.681	3.91	4.03	0.326	1.00	0.421	0.198

	After UV			
Sample	P_S (μC cm^{-2})	P_R (μC cm^{-2})	E_S (mJ cm^{-3})	η (%)
[a]IP33	0.933	1.018	8.27	4.63
[b]IP31	−0.037	0.662	4.03	3.32
[c]5%-IP33	0.185	0.141	2.45	8.49
[d]5%-IP31	0.339	0.549	4.06	3.17

our bent-core based materials. Alternatively, the application of UV irradiation can destabilise the liquid crystalline order by an increase of curved *cis*-azobenzene isomers that are not compatible with the mesophase, and promote phase transitions.[73,74] It is then interesting to study the coupled effect of electrical fields and light irradiation on the phase structure of our bent-core based samples. Even though the experiments in Fig. 10 did not result in phase transitions, we have found that isothermal clearing from the mesophases can occur under certain conditions near the clearing point, T_{cl} (up to T–T_{cl} = −7 K). Due to the high clearing temperatures of these compounds, the *trans*-to-*cis* equilibrium is displaced towards the thermal back isomerisation and the formation of *trans* isomers, and very high light intensities are required to yield isothermal isotropisation (>1000 mW cm^{-2}).

Whilst phase transitions from ordered mesophases to disordered melts are common, see for example,[75,76] we now investigate whether a combination of light and electrical fields could promote an isothermal transition between different mesophases. Even though the columnar phase cannot be transformed isothermally into a smectic phase by the mere application of electrical fields,[28,62] our results in Fig. 6 have already suggested the formation of some layered ordering after the application of several hysteresis cycles. Alternatively, we have found a phase transition route for IP31 consisting of: first promoting isotropisation of its columnar phase by irradiation with strong UV light intensities near the clearing point, T–T_{cl} =−4 K, Fig. 11(a), followed by the application of a strong electrical field (in the dark), which yields a new granular texture consistent with smectic phases, Fig. 11(b).

To our knowledge, this could be the first example when a smectic phase is formed isothermally from a columnar phase (through an isotropic melt) in a bent-core based material.[77] By restricting the area exposed to electrical fields, we have obtained cells with coexisting (induced) smectic and (original) columnar phases separated by an interface, see Fig. 12. This phenomenon can be very useful to build grating devices with regions having different physical properties, by using photomasks.[78] We note that, either the application of electrical fields when cooling from the isotropic melt (no UV irradiation), or the removal of the electrical fields when reforming the mesophase after UV irradiation (no electrical field in the dark), on their own, only lead to the reappearance of columnar phases in IP31.

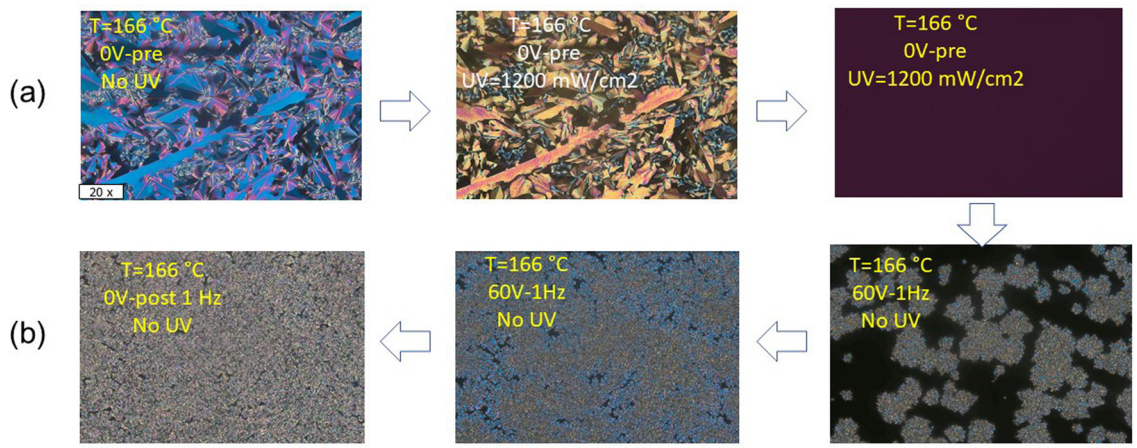

Fig. 11 Polarised optical micrographs obtained for IP31 at T = 166 °C: (a) application of UV irradiation (1200 mW cm^{-2}; 365 nm), followed by (b) strong electrical fields (75 kV cm^{-1}), resulting in a granular smectic phase.

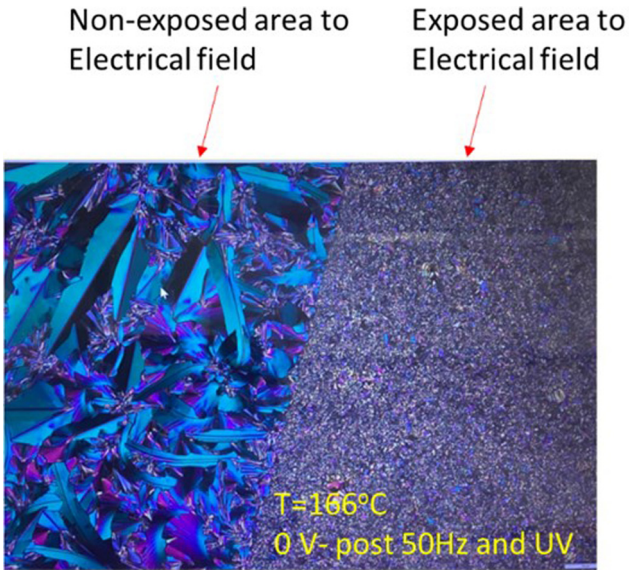

Fig. 12 Polarised optical micrograph obtained for a IP31 sample following the UV and electrical fields cycle described in Fig. 11, resulting in coexisting regions of columnar and smectic phases.

4. Conclusions

We have demonstrated the potential of the five bent-core based materials under study to transfer or store electrical energy, by a combination of dielectric, ferroelectric, and relaxor behaviour. Their response to electrical stimuli is related to Goldstone-modes of molecular reorientational motions within the smectic or columnar fields, activated at low frequencies ($\sim$1 Hz).

In addition, the presence of chromophore groups in pristine materials or in mixtures has been used as a mechanism to harvest light energy, by triggering *trans*-to-*cis* photoisomerisation of azobenzene groups. Light irradiation enhances conductivity and polarisation, even at low concentrations of photochromic groups. The ultimate reason for such improvement is unclear, due to the low yield of *cis*-azobenzene isomers expected at high temperatures, and will be the object of further research. We hypothesise that the disruption of the local liquid crystalline packing by the curved geometry of the *cis*-isomers can promote motions that facilitate the electrical signal in these materials. However, we cannot rule out that the concentration of *cis*-isomers near the glass electrodes enhances the alignment in smectic materials. Our next steps to design functional energy storage materials will involve controlling the size of the polar regions to increase polarisation and promoting steric hindrance that inhibit certain rotational mechanisms necessary for the *cis*-to-*trans* back isomerisation of the azobenzenes. Some of these facts could explain the UV-vis response observed by the films in the mesophase, and could ultimately lead to irreversible structural and excited states.

The induction of an isothermal columnar to smectic phase transition in IP31 (*via* isotropisation) by a combination of light and electrical fields is a promising tool to develop electric response through the formation (and control) of layered nanostructures. Examples in the literature of light-induced ordered phases are rare, normally attributed to nanophase separation,[79] hence our results can be applied to other fields of liquid crystals, soft matter, and nanotechnology.

Conflicts of interest

There are no conflicts to declare.

Acknowledgements

IDC would like to thank the Universitat Politècnica de València (UPV), for the FPI grant (PAID-2019-SP20190013), the Generalitat Valenciana (GVA) and the European Social Fund (ESF), for the FPI grant (ACIF/2020/233) and the mobility grant (CIBEFP/2021/53). NFKA would like to thank Universiti Teknologi MARA (UiTM) for sponsoring her academic sabbatical leave and allowing her to work on this project. AMF would like to thank the Carnegie Trust for the Universities of Scotland, for the Research Incentive Grant RIG008586, the Royal Society and Specac Ltd., for the Research Grant RGS\R1\201397, the Royal Society of Chemistry for the award of a mobility grant (M19-0000), and the Scottish Government and the Royal Society of Edinburgh for the award of a SAPHIRE project. The authors from INMA greatly appreciate financial support from projects of the Spanish Government PGC2018-093761-B-C31 [MCIU/AEI/FEDER, UE] and the Gobierno de Aragón/FEDER (research group E47_20R). Thanks are given to the nuclear magnetic resonance, mass spectrometry, and thermal analysis services of the INMA (Univ. Zaragoza-CSIC)

References

1 International Energy Agency, *Global Energy Review 2020*, 2020, IEA, Paris.
2 Y. Shen and I. Dierking, Perspectives in Liquid-Crystal-Aided Nanotechnology and Nanoscience, *Appl. Sci.*, 2019, **9**(12), 2512.
3 A. Martinez-Felipe, Liquid crystal polymers and ionomers for membrane applications, *Liq. Cryst.*, 2011, **38**(11–12), 1607–1626.
4 P. K. Bhowmik, *et al.*, Ionic liquid crystals: Synthesis and characterization via NMR, DSC, POM, X-ray diffraction and ionic conductivity of asymmetric viologen bistriflimide salts, *J. Mol. Liq.*, 2021, **328**, 115370.
5 A. Natansohn and P. Rochon, Photoinduced motions in azo-containing polymers, *Chem. Rev.*, 2002, **102**(11), 4139–4175.
6 H. M. D. Bandara and S. C. Burdette, Photoisomerization in different classes of azobenzene, *Chem. Soc. Rev.*, 2012, **41**(5), 1809–1825.
7 G. S. Hartley, The cis-form of azobenzene, *Nature*, 1937, **140**, 281.
8 A. L. Leistner and Z. L. Pianowski, Smart Photochromic Materials Triggered with Visible Light, *Eur. J. Org. Chem.*, 2022, e202101271.

9 G. A. Leith, *et al.*, Dynamically Controlled Electronic Behavior of Stimuli-Responsive Materials: Exploring Dimensionality and Connectivity, *Adv. Energy Mater.*, 2022, **12**(4), 2100441.
10 H. Sugiyama, S. Sato and K. Nagai, Photo-isomerization, photodimerization, and photodegradation polyimides for a liquid crystal alignment layer, *Polym. Adv. Technol.*, 2022, **33**(7), 2113–2122.
11 B. Zhang, Y. Y. Feng and W. Feng, Azobenzene-Based Solar Thermal Fuels: A Review, *Nano-Micro Lett.*, 2022, **14**(1), 138.
12 A. R. Ibrahim, *et al.*, p-Methoxy Azobenzene Terpolymer as a Promising Energy-Storage Liquid Crystal System, *J. Phys. Chem. C*, 2021, **125**(41), 22472–22482.
13 T. Niori, *et al.*, Distinct ferroelectric smectic liquid crystals consisting of banana shaped achiral molecules, *J. Mater. Chem.*, 1996, **6**(7), 1231–1233.
14 J. Etxebarria and M. B. Ros, Bent-core liquid crystals in the route to functional materials, *J. Mater. Chem.*, 2008, **18**(25), 2919–2926.
15 H. Takezoe and Y. Takanishi, Bent-core liquid crystals: Their mysterious and attractive world, *Jpn. J. Appl. Phys., Part 1*, 2006, **45**(2A), 597–625.
16 C. Tschierske, Development of Structural Complexity by Liquid-Crystal Self-assembly, *Angew. Chem., Int. Ed.*, 2013, **52**(34), 8828–8878.
17 R. A. Reddy and C. Tschierske, Bent-core liquid crystals: polar order, superstructural chirality and spontaneous desymmetrisation in soft matter systems, *J. Mater. Chem.*, 2006, **16**(10), 907–961.
18 A. Eremin and A. Jakli, Polar bent-shape liquid crystals – from molecular bend to layer splay and chirality, *Soft Matter*, 2013, **9**(3), 615–637.
19 H. Takezoe, Polar liquid crystals – ferro, antiferro, banana, and columnar, *Mol. Cryst. Liq. Cryst.*, 2017, **646**(1), 46–65.
20 K. V. Le, H. Takezoe and F. Araoka, Chiral Superstructure Mesophases of Achiral Bent-Shaped Molecules – Hierarchical Chirality Amplification and Physical Properties, *Adv. Mater.*, 2017, **29**(25), 1602737.
21 M. Hird, Ferroelectricity in liquid crystals-materials, properties and applications, *Liq. Cryst.*, 2011, **38**(11–12), 1467–1493.
22 D. R. Link, *et al.*, Spontaneous formation of macroscopic chiral domains in a fluid smectic phase of achiral molecules, *Science*, 1997, **278**(5345), 1924–1927.
23 M. Gong, *et al.*, Optimizing energy harvesting performance of silicone elastomers by molecular grafting of azobenzene to the macromolecular network, *RSC Adv.*, 2021, **11**(31), 19088–19094.
24 S. M. Alauddin, *et al.*, The role of conductivity and molecular mobility on the photoanisotropic response of a new azo-polymer containing sulfonic groups, *J. Photochem. Photobiol., A*, 2020, **389**, 112268.
25 G. G. Nair, *et al.*, Effect of light on the polarization of a banana-shaped achiral compound doped with a photoactive azobenzene material, *J. Appl. Phys.*, 2001, **90**(1), 48–52.
26 M. Martinez-Abadia, *et al.*, Photoresponsive Cyanostilbene Bent-Core Liquid Crystals as New Materials with Light-Driven Modulated Polarization, *Adv. Mater.*, 2016, **28**(31), 6586–6591.
27 M. Martinez-Abadia, *et al.*, Multiresponsive luminescent dicyanodistyrylbenzenes and their photochemistry in solution and in bulk, *J. Mater. Chem. C*, 2016, **4**(14), 2886–2893.
28 C. L. Folcia, *et al.*, Achiral bent-core liquid crystals with azo and azoxy linkages: Structural and nonlinear optical properties and photoisomerization, *Chem. Mater.*, 2006, **18**(19), 4617–4626.
29 J. Ortega, *et al.*, Electric-field-induced phase transitions in bent-core mesogens determined by x-ray diffraction, *Phys. Rev. E: Stat., Nonlinear, Soft Matter Phys.*, 2011, **84**(2), 021707.
30 M. Martinez-Abadia, *et al.*, Cyanostilbene bent-core molecules: a route to functional materials, *J. Mater. Chem. C*, 2015, **3**(13), 3038–3048.
31 D. Zaton, *et al.*, Photo-driven effects in twist-bend nematic phases: Dynamic and memory response of liquid crystalline dimers, *J. Mol. Liq.*, 2021, **344**, 117680.
32 I. C. Pintre, *et al.*, Liquid crystalline and nonlinear optical properties of bent-shaped compounds derived from 3,4′-biphenylene, *J. Mater. Chem.*, 2007, **17**(21), 2219–2227.
33 D. Shen, *et al.*, Molecular Design of Nonchiral Bent-Core Liquid Crystals with Antiferroelectric Properties, *J. Am. Chem. Soc.*, 2000, **122**(8), 1593–1601.
34 A. Martinez-Felipe, C. T. Imrie and A. Ribes-Greus, Study of Structure Formation in Side-Chain Liquid Crystal Copolymers by Variable Temperature Fourier Transform Infrared Spectroscopy, *Ind. Eng. Chem. Res.*, 2013, **52**(26), 8714–8721.
35 L. Guo, *et al.*, Transition between two orthogonal polar phases in symmetric bent-core liquid crystals, *Soft Matter*, 2011, **7**(6), 2895–2899.
36 S. U. Vallerien, *et al.*, Field-Dependent Soft and Goldstone Mode in a Ferroelectric Liquid-Crystal as Studied by Dielectric-Spectroscopy, *Phys. Lett. A*, 1989, **138**(4–5), 219–222.
37 L. F. Guo, *et al.*, Ferroelectric behavior of orthogonal smectic phase made of bent-core molecules, *Phys. Rev. E: Stat., Nonlinear, Soft Matter Phys.*, 2011, **84**(3), 031706.
38 F. Gouda, K. Skarp and S. T. Lagerwall, Dielectric studies of the soft mode and Goldstone mode in ferroelectric liquid crystals, *Ferroelectrics*, 1991, **113**(1), 165–206.
39 J. Ortega, *et al.*, Electric-field-induced B-1-B-2 transition in bent-core mesogens, *Phys. Rev. E: Stat., Nonlinear, Soft Matter Phys.*, 2004, **69**(1), 011703.
40 A. V. Gorbunov, *et al.*, True ferroelectric switching in thin films of trialkylbenzene-1,3,5-tricarboxamide (BTA), *Phys. Chem. Chem. Phys.*, 2016, **18**(34), 23663–23672.
41 S. Mohd Alauddin, *et al.*, Liquid Crystalline Copolymers Containing Sulfonic and Light-Responsive Groups: From Molecular Design to Conductivity, *Molecules*, 2020, **25**(11), 2579.
42 S. M. Alauddin, *et al.*, New side-chain liquid crystalline terpolymers with anhydrous conductivity: Effect of azobenzene substitution on light response and charge transfer, *Eur. Polym. J.*, 2021, **146**, 110246.

43 L. Vanti, *et al.*, *Ionically conducting and photoresponsive liquid crystalline terpolymers: Towards multifunctional polymer electrolytes*, 2018, pp. 124–132.
44 A. Martinez-Felipe, *et al.*, Characterization of Functionalized Side-Chain Liquid Crystal Methacrylates Containing Non-mesogenic Units by Dielectric Spectroscopy, *Ind. Eng. Chem. Res.*, 2013, **52**(26), 8722–8731.
45 K. A. Mauritz and R. B. Moore, State of understanding of Nafion, *Chem. Rev.*, 2004, **104**(10), 4535–4585.
46 A. C. Luntz and B. D. McCloskey, Nonaqueous Li-Air Batteries: A Status Report, *Chem. Rev.*, 2014, **114**(23), 11721–11750.
47 K. Kishimoto, *et al.*, Nano-segregated polymeric film exhibiting high ionic conductivities, *J. Am. Chem. Soc.*, 2005, **127**(44), 15618–15623.
48 A. Concellon, *et al.*, Proton conductive ionic liquid crystalline poly(ethyleneimine) polymers functionalized with oxadiazole, *RSC Adv.*, 2018, **8**(66), 37700–37706.
49 A. Concellon, *et al.*, Proton-conductive materials formed by coumarin photocrosslinked ionic liquid crystal dendrimers, *J. Mater. Chem. C*, 2018, **6**(5), 1000–1007.
50 T. Kobayashi, *et al.*, Development of Glassy Bicontinuous Cubic Liquid Crystals for Solid Proton-Conductive Materials, *Adv. Mater.*, 2017, **29**(4), 1604429.
51 T. Liang, *et al.*, Anisotropic Dye Adsorption and Anhydrous Proton Conductivity in Smectic Liquid Crystal Networks: The Role of Cross-Link Density, Order, and Orientation, *ACS Appl. Mater. Interfaces*, 2017, **9**(40), 35218–35225.
52 G. S. McHattie, C. T. Imrie and M. D. Ingram, Ionically conducting side chain liquid crystal polymer electrolytes, *Electrochim. Acta*, 1998, **43**(10–11), 1151–1154.
53 L. Vanti, *et al.*, Ionically conducting and photoresponsive liquid crystalline terpolymers: Towards multifunctional polymer electrolytes, *Eur. Polym. J.*, 2018, **109**, 124–132.
54 J. S. Yang, *et al.*, New anhydrous proton exchange membranes based on fluoropolymers blend imidazolium poly (aromatic ether ketonejs for high temperature polymer electrolyte fuel cells, *Int. J. Hydrogen Energy*, 2018, **43**(17), 8464–8473.
55 X. H. Yang, *et al.*, A unidomain membrane prepared from liquid-crystalline poly(pyridinium 4-styrene sulfonate) for anhydrous proton conduction, *J. Membr. Sci.*, 2017, **523**, 355–360.
56 S. Yuan, *et al.*, Poly(imide benzimidazole)s for high temperature polymer electrolyte membrane fuel cells, *J. Membr. Sci.*, 2014, **454**, 351–358.
57 M. Cestari, *et al.*, Phase behavior and properties of the liquid-crystal dimer 1″,7″-bis(4-cyanobiphenyl-4′-yl) heptane: A twist-bend nematic liquid crystal, *Phys. Rev. E: Stat., Nonlinear, Soft Matter Phys.*, 2011, **84**(3), 031704.
58 B. Robles-Hernandez, *et al.*, Twist, tilt, and orientational order at the nematic to twist-bend nematic phase transition of 1″,9″-bis(4-cyanobiphenyl-4′-yl) nonane: A dielectric, H-2 NMR, and calorimetric study, *Phys. Rev. E: Stat., Nonlinear, Soft Matter Phys.*, 2015, **92**(6), 062505.
59 R. Walker, *et al.*, The Chiral Twist-Bend Nematic Phase (N*(TB)), *Chem. – Eur. J.*, 2019, **25**(58), 13329–13335.
60 O. Elamain, *et al.*, Field-induced optically isotropic state in bent core nematic liquid crystals: unambiguous proof of field-induced optical biaxiality, *J. Phys. D: Appl. Phys.*, 2013, **46**(45), 455101.
61 D. Wiant, *et al.*, Nonstandard electroconvection in a bent-core nematic liquid crystal, *Phys. Rev. E: Stat., Nonlinear, Soft Matter Phys.*, 2005, **72**(4), 041712.
62 J. Martinez-Perdiguero, *et al.*, Pseudolayered structure of the columnar B1 phase of bent-core liquid crystals, *Phys. Rev. E: Stat., Nonlinear, Soft Matter Phys.*, 2010, **82**(4), 041706.
63 A. Jakli, Liquid crystals of the twenty-first century – nematic phase of bent-core molecules, *Liq. Cryst. Rev.*, 2013, **1**(1), 65–82.
64 M. M. El-Desoky, *et al.*, Relaxor ferroelectric-like behavior in 10PbTiO(3)-10Fe(2)O(3)-30V(2)O(5)-50B(2)O(3) glass for energy storage applications, *J. Mater. Sci.: Mater. Electron.*, 2021, **32**(17), 22408–22416.
65 W. J. Shi, *et al.*, Relaxor antiferroelectric-like characteristic boosting enhanced energy storage performance in eco-friendly $(Bi_{0.5}Na_{0.5})TiO_3$-based ceramics, *J. Eur. Ceram. Soc.*, 2022, **42**(11), 4528–4538.
66 G. S. Kumar and D. C. Neckers, Photochemistry of Azobenzene-Containing Polymers, *Chem. Rev.*, 1989, **89**(8), 1915–1925.
67 I. Chaganava, *et al.*, Induction of the vector polyphotochromism in side-chain azopolymers, *J. Photochem. Photobiol., A*, 2018, **354**, 70–77.
68 A. Concellon, *et al.*, Light-Responsive Self-Assembled Materials by Supramolecular Post-Functionalization via Hydrogen Bonding of Amphiphilic Block Copolymers, *Macromolecules*, 2016, **49**(20), 7825–7836.
69 S. K. Prasad, *et al.*, A soft-bent dimer composite exhibiting twist-bend nematic phase: Photo-driven effects and an optical memory device, *Appl. Phys. Lett.*, 2018, **112**(25), 253701.
70 S. K. Prasad, *et al.*, Photoinduced effects in nematic liquid crystals, *Phase Transitions*, 2005, **78**(6), 443–455.
71 J. Casellas, M. J. Bearpark and M. Reguero, Excited-State Decay in the Photoisomerisation of Azobenzene: A New Balance between Mechanisms, *Chem. Phys. Chem.*, 2016, **17**(19), 3068–3079.
72 A. Kumar, *et al.*, Composition dependent ferro-piezo hysteresis loops and energy density properties of mechanically activated $(Pb_{1-x}La_x)(Zr_{0.60}Ti_{0.40})O$-3 ceramics, *Appl. Phys. A: Mater. Sci. Process.*, 2020, **126**(3), 175.
73 S. K. Prasad, Photo-Stimulated and Photo-Suppressed Phase Transitions, *Mol. Cryst. Liq. Cryst.*, 2009, **509**, 1059–1069.
74 D. A. Paterson, *et al.*, Reversible Isothermal Twist-Bend Nematic-Nematic Phase Transition Driven by the Photoisomerization of an Azobenzene-Based Nonsymmetric Liquid Crystal Dinner, *J. Am. Chem. Soc.*, 2016, **138**(16), 5283–5289.
75 S. Shruthi, *et al.*, Influence of linking units on the photo responsive studies of azobenzene liquid Crystals: Application in optical storage devices, *J. Mol. Liq.*, 2021, **339**, 116744.

76 R. S. Hegde, *et al.*, Influence of alkyl and alkoxy groups on photoresponsive behaviour of bent-core azo mesogens: Synthesis, mesomorphic and photoswitching properties, *J. Mol. Liq.*, 2020, **309**, 113091.
77 M. Alaasar, Azobenzene-containing bent-core liquid crystals: an overview, *Liq. Cryst.*, 2016, **43**(13–15), 2208–2243.
78 N. Begum, *et al.*, Photoswitchable Bent-Core Nematic Liquid Crystals with Methylated Azobenzene Wing Exhibiting Optic-Field-Enhanced Freedericksz Transition Effect, *J. Phys. Chem. C*, 2020, **124**(1), 874–885.
79 S. K. Prasad, G. G. Nair and G. Hegde, Dynamic self-assembly of the liquid-crystalline smectic A phase, *Adv. Mater.*, 2005, **17**(17), 2086–2091.